Thin Solid Films 544 (2013) 197–200

Contents lists available at ScienceDirect

Thin Solid Films

journal homepage: www.elsevier.com/locate/tsf

Multi-component transparent conductive oxide films on polyimide substrate prepared by radio frequency magnetron sputtering

YanWen Zhou [a,*], Xi Liu [a], YunHua Lu [b], Zhizhi Hu [b], ChaoKui Zhang [a], FaYu Wu [a]

[a] School of Materials and Metallurgy, University of Science and Technology Liaoning, No. 185 Qianshan Rd., Hi-tech District, Anshan, Liaoning 114051, China
[b] School of Chemical Engineering, University of Science and Technology Liaoning, No. 185 Qianshan Rd., Hi-tech District, Anshan, Liaoning 114051, China

ARTICLE INFO

Available online 10 April 2013

Keywords:
Multi-component TCO film
Flexible organic transparent substrate
RF magnetron sputtering
PI

ABSTRACT

Multi-component tin, zinc and cadmium oxide ($Sn_xZn_yCd_{1-x-y}O$) transparent conductive oxide coatings with high transparency and charge carrier mobility were prepared on polyimide substrates by radio frequency magnetron sputtering from powder targets. The films were columnar in morphological, but with defects present. The microstructure was nano-crystalline for the film containing the highest Cd content, and a mixture of amorphous and nano-crystalline for other films. The average transmittance within the visible wavelength range improved from 70% to 90% with decreasing Cd or Sn content in the films. The charge carrier concentrations of the films were of the order of 10^{16} cm^{-3}, and the highest mobility reached 31 cm^2/V s. This initial study of $Sn_xZn_yCd_{1-x-y}O$ films on polyimide substrates shows promise for applications, such as flexible thin film transistors.

1. Introduction

With the development of opto-electronic devices, such as photovoltaic solar cells, flat panel devices, thin film transistors (TFT) and light emitting diodes etc., transparent conductive oxide (TCO) coatings on flexible transparent substrates becoming more and more attractive [1–7]. Apart from doped oxide films for passive applications [2–5,8], many studies of multi-component TCO films for active applications have been carried out [1,6,7,9,10]. Most multi-component oxide coatings have amorphous structures, which offer not only optical transparency, but also high carrier mobility and phase stability due to low self-trapping of ns electrons and the absence of grain boundaries [1,11–13]. The amorphous semiconductive materials involved in α-TFTs are a mixture of the heavy-metal oxides, such as indium, gallium, zinc, tin, cadmium and strontium oxides [12–18]. Among those oxides, indium oxide (In_2O_3) is believed to have excellent optical and electrical properties, but it is a scarce resource and therefore, very expensive. Cadmium oxide (CdO) offers not only conductivity as high as that of In_2O_3, but also the highest carrier mobility (up to 200 cm^2/V s) [18]. Of course, the heavy metal element Cd should be used carefully and sparingly due to its toxicity. Zinc oxide (ZnO) and tin oxide (SnO_2) are the most commonly used TCO materials with high transparency and large band gaps (>3.2 and 3.6 eV for ZnO and SnO_2 films, respectively) in comparison with the band gaps of CdO (direct band gap, 2.3 eV; indirect band gaps, 0.8 and 1.1 eV) [2,7,19–24]. Therefore, SnO_2, ZnO and CdO were chosen in this study due to their low costs and the wide range of their electrical and optical properties.

There are many techniques available to prepare multi-component TCO films, for example, magnetron sputtering, pulse laser deposition, chemical vapor deposition, sol–gel, spray-pyrolysis, inkjet-printing and combinatorial approaches [3,6,17,20,21,25–31]. To produce the required properties, the coated substrates often have to bear either high deposition temperatures or post-deposition annealing. Magnetron sputtering is the process of choice for preparing the films at low temperature, and is suitable for use on flexible organic substrates. Closed-field unbalanced magnetron sputtering from powder targets in pulsed DC mode has been used by the authors in recent years to deposit multi-component materials [27,32–35]. Powder targets offer the advantages of low cost and easily variable coating composition [27,33,35]. In this study, a radio frequency (RF) discharge, which produced a high plasma density, but low ion energy, was used instead of pulsed DC to deposit multi-component films on the flexible polyimide substrate. The polyimide (PI) substrate film, produced by the University of Science and Technology Liaoning, has a glass transition temperature (T_g) and transparency within the visible range as high as 294 °C and 90%, respectively.

2. Experimental details

The $Sn_xZn_yCd_{1-x-y}O$ coatings were deposited in a rig specifically designed for powder target use. The substrate holder was positioned directly above the magnetron, at a separation of 150 mm. Before mounting on the substrate holder, the substrates (PI and glass slides for comparison purposes) were ultrasonically cleaned in alcohol. The magnetron was driven by an Advanced Energy RFX600 13.56 MHz RF power supply. The 99.99% pure SnO_2, ZnO and CdO powders were mixed and blended at appropriate atomic ratios, ready for using as targets. The mixed powder was distributed uniformly across the surface

* Corresponding author. Tel.: +86 13998097083; fax: +86 412 5929525.
E-mail address: zhouyanwen@yahoo.com (Y. Zhou).

0040-6090/$ – see front matter © 2013 Elsevier B.V. All rights reserved.
http://dx.doi.org/10.1016/j.tsf.2013.03.122

of a copper backing plate on the magnetron and lightly tamped down. No further processes, such as sintering, were involved in target production. The rig was then evacuated to a base pressure of lower than 3×10^{-3} Pa and backfilled with Argon gas to a pressure of 0.2 Pa. The substrates were RF sputter cleaned at 100 W for 15 min. The coatings were then deposited at 100 W RF power for 9 h to avoid PI deformation. The different target compositions tested are listed in Table 1. Also, additional pure SnO_2, ZnO and CdO coatings were deposited at 200 W and their deposition rates calculated to be 185, 80 and 488 nm/h, respectively.

The cross-sectional composition of the film was probed and analyzed by Auger electron spectroscopy (AES ULVAC-PHI 700). A silicon oxide film on a silicon wafer was used as a standard sample, which was sputtered by an Ar^+ gun at a pressure of 5.2×10^{-7} Pa. The structures of the coatings were subsequently characterized by transmission electron microscopy (TEM JEM 2100) at 200 kV working voltage, atomic force microscopy (AFM CSPM 3000) by contact mode, X-ray diffraction (XRD X'PERT PRO) scanning with copper Kα radiation in θ–2θ mode. The coatings were gently scratched off the PI substrates using a surgical blade. The pieces were then placed into pure alcohol and vibrated by an ultrasonic machine to disperse the coating chips. A carbon supported copper grid was used to collect the chips to form the TEM samples. Coating thicknesses were measured by an Afar-Step IQ Surface Profiler. The electrical and optical properties were investigated according to the Van-der Pauw method by using a SWIN Hall 8800 at room temperature and a UV-2802S spectrophotometer, respectively.

3. Results and discussion

3.1. Coating composition

One coating, deposited from a target with a compositional ratio of Sn:Zn:Cd = 2:2:1, was chosen to be analyzed by AES and the compositional depth profiles are shown in Fig. 1. It can be seen that the oxygen component in the film did not reach the full stoichiometry value, which often happens when the coatings of this type are prepared in a pure Ar atmosphere [27,32]. The depth profiles for the metallic elements can be divided into two parts. The top portion of the film (sputtering time from 0 to 1.25 min) has a Sn:Zn:Cd ratio of 2:2:0.9, which is very similar to the composition of the target. In the lower portion of the film (sputtering time from 1.25 to 2.5 min), i.e., the layer deposited first, the coating composition was Cd rich, and Sn and Zn poor compared to that of the target. The possible reasons for this are as follow: CdO has the highest sputtering rate, as determined during the pure target deposition rate investigation referred to earlier. Thus the initial sputtering rate of CdO from the target surface would be faster than those of SnO_2 and ZnO and the surface of the target would become depleted of CdO. Eventually equilibrium is reached and the composition of the film becomes similar to that of the target.

3.2. Coating structure

Fig. 2 shows the morphological structure of the $Sn_xZn_yCd_{1-x-y}O$ films from AFM analysis. The coatings both on polyimide and glass

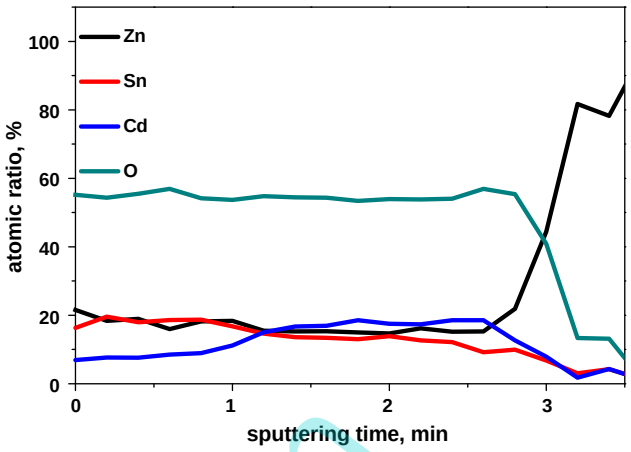

Fig. 1. Cross-sectional composition of the $Sn_{0.4}Zn_{0.4}Cd_{0.2}O$ film by AES.

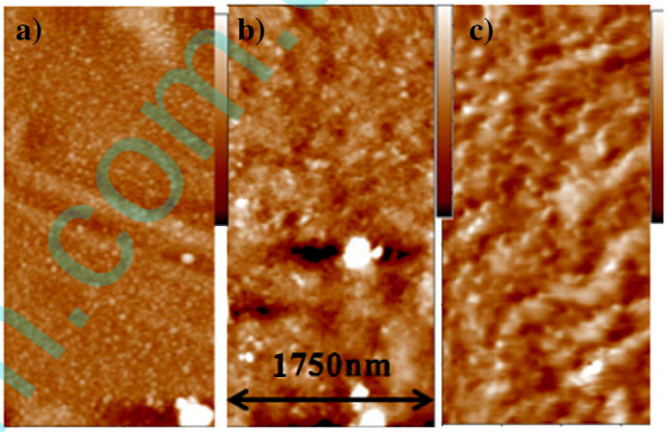

Fig. 2. Morphological structures by AFM: a) $Sn_{0.2}Zn_{0.2}Cd_{0.6}O$ on PI, the z-bar was 0–30 nm; b) $Sn_{0.4}Zn_{0.4}Cd_{0.2}O$ on PI, the z-bar 0–8 nm; and c) $Sn_{0.4}Zn_{0.2}Cd_{0.4}O$ on glass, the z-bar 0–10 nm.

slides were columnar, but with defects present in the coatings on PI. The roughness of the films was calculated by CSPM image analyzer software. The root mean square roughness of the films was about 1 nm except for the film with the highest Cd content (RMS = 4.15 nm), which indicated that the surfaces of the multi-component coatings were generally very smooth. The maximum heights in the AFM images of the films in Fig. 2a) and b) were 30 and 8 nm because they were enlarged by defects in the films. There might be two possible reasons to have defects of the films on PI: PI substrates are hydrophobic, which reduces the adhesion of the coating to the PI; the coefficient of thermal expansion of the PI was very different to that of the coating, and the resulting interfacial stresses may have broken the coating bond [2]. In Fig. 3, it can be seen that the domain sizes of the

Table 1
Optical and electrical properties of the $Sn_xZn_yCd_{1-x-y}O$ films on PI and glass.

Sample no.	Targets Sn:Zn:Cd (atomic ratio)	Film thickness nm	Cut-off points nm	Concentration of charge carriers $\times 10^{16}$ (cm^{-3})	Mobility $cm^2/V\ s$	Resistivity Ω cm	
						Polyimide substrate	Glass $\times 10^{-2}$
1	1:1:3	329	325	1.36	**31**	14.9	0.14
2	1:2:2	159	311	**75.7**	**0.856**	9.63	17.2
3	2:1:2	198	312	2.95	**25.2**	8.40	0.98
4	1:3:1	154	303	8.25	9.91	**7.46**	**3110**
5	2:2:1	155	301	7.21	10.6	8.16	2.11
6	3:1:1	325	300	5.31	6.81	17.2	0.29

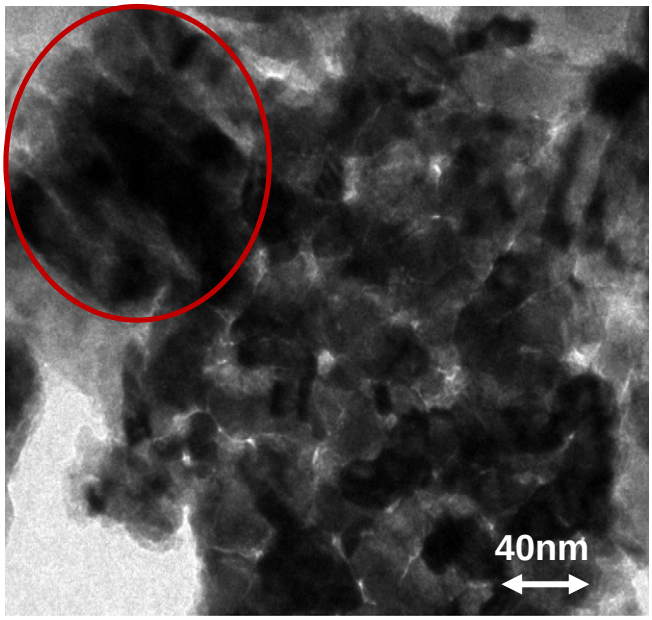

Fig. 3. TEM micrograph of a $Sn_{0.2}Zn_{0.2}Cd_{0.6}O$ film showing a columnar nano-crystalline region.

nano-crystalline regions of the coating are about 30–40 nm. Also, the columnar structures can be identified in the circled area. This micrograph was taken from the sample with the highest Cd content. All other films were a mixture of nano-crystalline and amorphous regions.

The main preferred orientation of CdO (200) was visible in the XRD pattern of the highest Cd content film (sample No.1), see Fig. 4. There were no obviously identifiable peaks in the other 5 XRD patterns, although low intensity diffraction peaks could be seen in some cases. This indicated a nano-crystalline structure for the film with the highest Cd ratio, and a mixture of amorphous and nano-crystalline structures or predominantly amorphous structures for the other films. The reason that the film with the highest Cd ratio had a nano-crystalline structure might be that CdO needs a much lower crystallization energy than those of SnO_2 and ZnO [36]. Of course, SnO_2 and ZnO crystal lattices may exist more or less in all multi-component $Sn_xZn_yCd_{1-x-y}O$ coatings. Anyway, it might be difficult to form long range atomic order in these coatings, because the three metallic atoms tend to replace the positions of each other in the lattice.

3.3. Optical properties

The average transmittance of the $Sn_xZn_yCd_{1-x-y}O$ films within the visible wavelength range varied from 70% to 90%, depending on coating composition (Fig. 5). The cut-off wavelengths listed in Table 1 and indicated in a ternary diagram in Fig. 6 are the intercepts of the tangents of the transmittance spectra at near ultraviolet regions, as determined using Origin 8.0 software. The transmittance increased as the Cd and Sn decreased in the films. The direct band gaps of intrinsic SnO_2, ZnO and CdO films were 3.6, 3.2 and 2.3 eV, which are in inverse proportion to the cut-off points of the optical spectra. Therefore, the cut-off point of SnO_2 film is the shortest in the optical spectra among these three oxide films, ZnO the second and CdO the longest. The cut-off points of the multi-component films shift towards shorter wavelengths as the Cd proportion decreases and the Sn proportion increases, and those of the films containing 20 at.% Sn are very similar in value. It can clearly be seen that the cut-off points of the films decreased as the compositions changed from the CdO corner to the SnO_2 and ZnO corners in the ternary diagram (Fig. 6). Therefore, it is easy to adjust the cut-off points (or band gaps) of the multi-component coatings by simply changing the ratios of the metallic components.

3.4. Electrical properties

The electrical properties of the $Sn_xZn_yCd_{1-x-y}O$ films on PI are summarized in Table 1, and indicated in ternary diagrams in Figs. 6 and 7. The resistivities of the films on glass slides measured by four point probes are also shown in Table 1. All films were n-type semiconductors and electrons were the free charge carriers. The charge carrier concentrations of the multi-component films on PI were in the range of 10^{16} cm^{-3}. Carrier mobilities of up to 31 $cm^2/V\,s$ could be seen from the film with the highest Cd content. Also, the carrier mobility of the $Sn_{0.4}Zn_{0.2}Cd_{0.4}O$ was over 25 $cm^2/V\,s$. The films containing high Cd had relatively low carrier concentrations and high carrier mobility. It can be seen in Figs. 6 and 7 that the multi-component films with long cut-off points, i.e. film compositions near the CdO corner of the ternary diagrams, had relatively low charge carrier concentrations and high mobilities. It has to be mentioned that the resistivity of the films on polyimide substrates were 3–4 orders higher than those on glass slides. The former were about 10 Ω cm, and the latter were in the range of 10^{-2} to 10^{-3} Ω cm. One reason for the big difference might be that defects existed in the films on PI, which trapped the electrons and blocked the transfer of the electrons within the films. The results

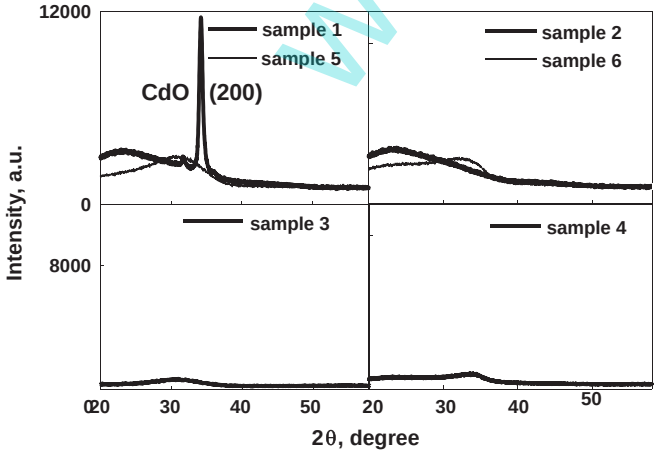

Fig. 4. θ–2θ XRD patterns of the $Sn_xZn_yCd_{1-x-y}O$ films.

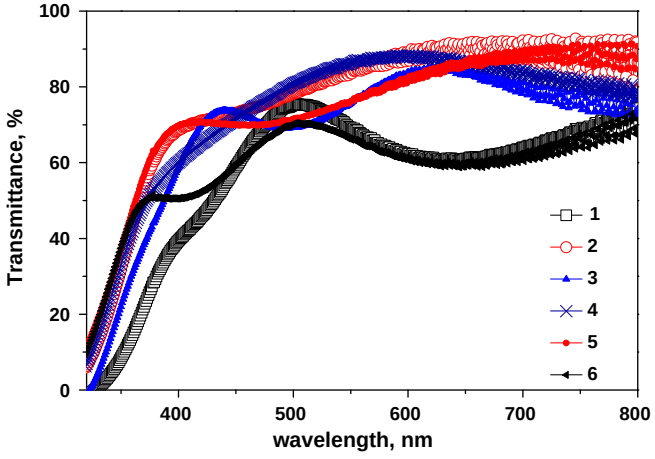

Fig. 5. Transmittance spectra of the $Sn_xZn_yCd_{1-x-y}O$ films on PI.

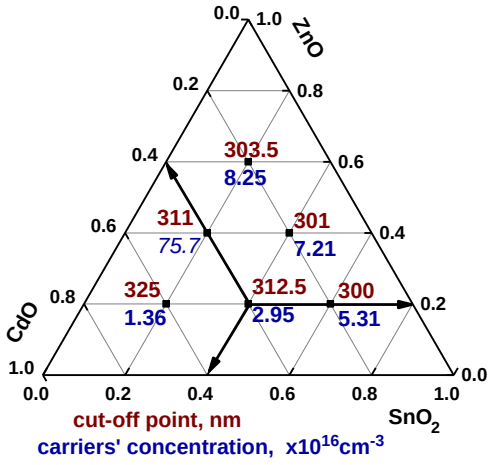

Fig. 6. Ternary diagram showing cut-off points and charge carrier concentrations of the $Sn_xZn_yCd_{1-x-y}O$ films.

of Sample No. 2 by Hall Effect measurement and Sample No. 4 by four point probe measurement were unusual and might not be accurate.

In general, the as-deposited $Sn_xZn_yCd_{1-x-y}O$ films on PI prepared by RF magnetron sputtering were produced with no melting and deformation of the substrate. The initial study of the films showed high transmittance, high charge carrier mobility and low carrier concentrations, which would be suitable for use as the active layer in devices, such as TFTs.

4. Conclusions

$Sn_xZn_yCd_{1-x-y}O$ films were deposited by RF sputtering from powder targets directly onto PI substrates with no melting or deformation of the substrate. The use of blended powder targets allowed a wide range of compositions to be studied efficiently and economically. Most of the $Sn_xZn_yCd_{1-x-y}O$ films were a mixture of amorphous and nano-crystalline structures, but defects were present in the films on PI. The $Sn_xZn_yCd_{1-x-y}O$ films were n-type semi-conductive TCOs. The transmittance of the films at a wavelength of 650 nm was up to 90%, the bulk charge carrier concentrations were about 10^{16} cm^{-3}, and the mobility reached 31 cm^2/V s. The mobility of the charge carriers was mainly contributed by the Cd component, and the transmittance of the films benefitted from the Zn and Sn components.

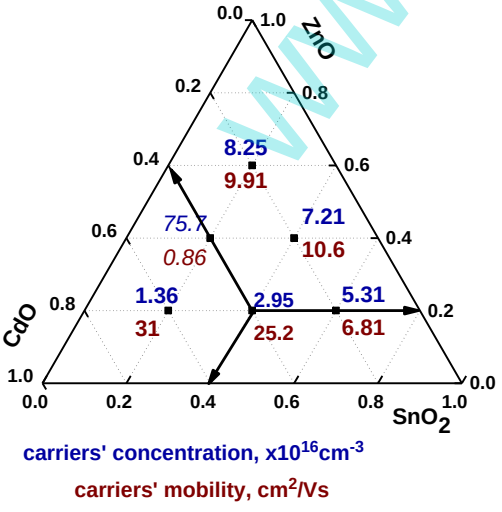

Fig. 7. Ternary diagram showing charge carrier concentrations and mobility of the $Sn_xZn_yCd_{1-x-y}O$ films.

Acknowledgments

This work is supported by National Natural Science Foundation of China in Nos. 50872048 and 51172101.

Thanks go to Alan Postill, my old colleague in the UK, and Professor Peter Kelly, my PhD supervisor, for their helps with both scientific and English corrections in this paper.

References

[1] J.S. Park, W.-J. Maeng, H.-S. Kim, J.-S. Park, Thin Solid Films 520 (2012) 1679.
[2] E. Fortunato, P. Nunes, A. Marques, D. Costa, H. Águas, I. Ferreira, M.E.V. Costa, M.H. Godinho, P.L. Almeida, J.P. Borges, R. Martins, Surf. Coat. Technol. 151–152 (2002) 247.
[3] V. Klykov, I. Strazdina, V. Kozlov, Surf. Coat. Technol. 211 (2012) 180.
[4] J.-W. Park, G. Kim, S.-H. Lee, E.-H. Kim, G.-H. Lee, Surf. Coat. Technol. 205 (2010) 915.
[5] I.S. Song, S.W. Heo, J.R. Ku, D.K. Moon, Thin Solid Films 520 (2012) 4068.
[6] D.-H. Kim, W.-J. Kim, S.J. Park, H.W. Choi, K.-H. Kim, Surf. Coat. Technol. 205 (Supplement 1) (2010) S324.
[7] D.Y. Lee, J.R. Lee, G.H. Lee, P.K. Song, Surf. Coat. Technol. 202 (2008) 5718.
[8] T. Minami, Thin Solid Films 516 (2008) 1314.
[9] H.S. Shin, B.D. Ahn, K.H. Kim, J.-S. Park, H.J. Kim, Thin Solid Films 517 (2009) 6349.
[10] J.C. Moon, F. Aksoy, H. Ju, Z. Liu, B.S. Mun, Curr. Appl. Phys. 11 (2011) 513.
[11] E. Fortunato, A. Gonçalves, A. Pimentel, P. Barquinha, G. Gonçalves, L. Pereira, I. Ferreira, R. Martins, Appl. Phys. A: Mater. Sci. Process. 96 (2009) 197.
[12] J. Robertson, R. Gillen, S.J. Clark, Thin Solid Films 520 (2012) 3714.
[13] S. Lee, H. Park, D.C. Paine, Thin Solid Films 520 (2012) 3769.
[14] D.H. Yoon, S.J. Kim, W.H. Jeong, D.L. Kim, Y.S. Rim, H.J. Kim, J. Cryst. Growth 326 (2011) 171.
[15] P. Carreras, A. Antony, F. Rojas, J. Bertomeu, Thin Solid Films 520 (2011) 1223.
[16] S.-M. Yoon, S.-W. Jung, S.-H. Yang, C.-W. Byun, C.-S. Hwang, S.-H. Ko Park, H. Ishiwara, Org. Electron. 11 (2010) 1746.
[17] A.A. Ziabari, F.E. Ghodsi, Thin Solid Films 520 (2011) 1228.
[18] T.J. Coutts, D.L. Young, X. Li, W.P. Mulligan, X. Wu, J. Vac. Sci. Technol. A 18 (2000) 2646.
[19] H.C. Ma Damisih, J.-J. Kim, H.Y. Lee, Thin Solid Films 520 (2012) 3741.
[20] J.H. Ko, I.H. Kim, D. Kim, K.S. Lee, T.S. Lee, B. Cheong, W.M. Kim, Appl. Surf. Sci. 253 (2007) 7398.
[21] X. Han, R. Liu, Z. Xu, Thin Solid Films 517 (2009) 5653.
[22] K. Abe, K. Takahashi, A. Sato, H. Kumomi, K. Nomura, T. Kamiya, H. Hosono, Thin Solid Films 520 (2012) 3791.
[23] H. Köhler, Solid State Commun. 11 (1972) 1687.
[24] J.C. Boettger, A.B. Kunz, Phys. Rev. B 27 (1983) 1359.
[25] R. Mamazza Jr., D.L. Morel, C.S. Ferekides, Thin Solid Films 484 (2005) 26.
[26] W.H. Jeong, G.H. Kim, D.L. Kim, H.S. Shin, H.J. Kim, M.-K. Ryu, K.-B. Park, J.-B. Seon, S.-Y. Lee, Thin Solid Films 519 (2011) 5740.
[27] P.J. Kelly, Y. Zhou, J. Vac. Sci. Technol. A 24 (2006) 1782.
[28] R. Kumaravel, V. Krishnakumar, K. Ramamurthi, E. Elangovan, M. Thirumavalavan, Thin Solid Films 515 (2007) 4061.
[29] A. Kurz, M.A. Aegerter, Thin Solid Films 516 (2008) 4513.
[30] H.-K. Kim, I.-K. You, J.B. Koo, S.-H. Kim, Surf. Coat. Technol. 211 (2012) 33.
[31] S.J.C. Irvine, D.A. Lamb, V. Barrioz, A.J. Clayton, W.S.M. Brooks, S. Rugen-Hankey, G. Kartopu, Thin Solid Films 520 (2011) 1167.
[32] Y. Zhou, P.J. Kelly, Thin Solid Films 469–470 (2004) 18.
[33] Y. Zhou, P. Kelly, Q.B. Sun, Thin Solid Films 516 (2008) 4030.
[34] Y. Wei, Z. Yan Wen, Z. Chun Yan, W. Fa Yu, L. Lin, Electronics and Optoelectronics (ICEOE), 2011 International Conference on, Dalian, Liaoning, 2011, p. V4-320.
[35] Y. Zhou, Ph.D. Thesis, University of Salford, Manchester, United Kingdom, 2005.
[36] Y.W. Zhou, F.Y. Wu, C.Y. Zheng, Chin. Phys. Lett. 28 (2011) 107307.